Article

Engineering InAsP/InP/ZnSe III–V Alloyed Core/Shell Quantum Dots for the Near-Infrared

Sang-Wook Kim, John P. Zimmer, Shunsuke Ohnishi,
Joseph B. Tracy, John V. Frangioni, and Moungi G. Bawendi

J. Am. Chem. Soc., **2005**, 127 (30), 10526-10532• DOI: 10.1021/ja0434331 • Publication Date (Web): 08 July 2005

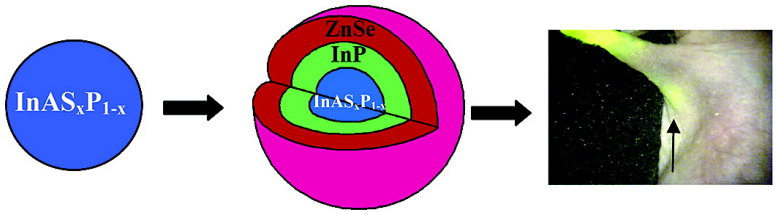

More About This Article

Additional resources and features associated with this article are available within the HTML version:

- Supporting Information
- Links to the 19 articles that cite this article, as of the time of this article download
- Access to high resolution figures
- Links to articles and content related to this article
- Copyright permission to reproduce figures and/or text from this article

View the Full Text HTML

J|A|C|S
ARTICLES
Published on Web 07/08/2005

Engineering $InAs_xP_{1-x}$/InP/ZnSe III−V Alloyed Core/Shell Quantum Dots for the Near-Infrared

Sang-Wook Kim,[†,§] John P. Zimmer,[†] Shunsuke Ohnishi,[‡] Joseph B. Tracy,[†] John V. Frangioni,[‡] and Moungi G. Bawendi*[,†]

Contribution from the Department of Chemistry, Massachusetts Institute of Technology, Cambridge, Massachusetts 02139, Division of Hematology/Oncology, Beth Israel Deaconess Medical Center, Boston, Massachusetts 02215, and Department of Molecular Science and Technology, Ajou University, Suwan 443-749, Korea

Received October 29, 2004; E-mail: mgb@mit.edu

Abstract: Quantum dots with a core/shell/shell structure consisting of an alloyed core of $InAs_xP_{1-x}$, an intermediate shell of InP, and an outer shell of ZnSe were developed. The $InAs_xP_{1-x}$ alloyed core has a graded internal composition with increasing arsenic content from the center to the edge of the dots. This compositional gradient results from two apparent effects: (1) the faster reaction kinetics of the phosphorus precursor compared to the arsenic precursor, and (2) a post-growth arsenic−phosphorus exchange reaction that increases the arsenic content. The cores have a zinc blend structure for all compositions and show tunable emission in the near-infrared (NIR) region. A first shell of InP leads to a red-shift and an increase in quantum yield. The final shell of ZnSe serves to stabilize the dots for applications in aqueous environments, including NIR biomedical fluorescence imaging. These NIR-emitting core/shell/shell $InAs_xP_{1-x}$/InP/ZnSe were successfully used in a sentinel lymph node mapping experiment.

Introduction

Semiconductor nanocrystal quantum dots (QDs) grown using wet chemical methods have attracted attention due to their application as tunable fluorescent markers in biological imaging and their potential uses in display devices, photovoltaics, and lasers.[1] Most studies have focused on QDs from the II−VI family. QDs from the III−V family are more difficult to synthesize using colloidal methods, and as a consequence only a relatively limited number of reports on InAs and InP QDs have been published.[2]

A wavelength range of particular interest for biomedical imaging is the near-infrared (NIR) between 800 and 900 nm, where absorption in tissue is minimal. We have recently demonstrated that QDs can be successfully applied in this context through in vivo vascular imaging and sentinel lymph node (SLN) mapping. These previous studies relied on type II NIR QDs[3] consisting of a CdTe core and a CdSe shell, where the band offsets between the two materials results in the electron preferring the shell while the hole prefers the core. Signatures of a type II QD are a longer radiative lifetime and the appearance of a red tail in the absorption spectrum. The longer radiative lifetime can result in lower quantum yields as the nonradiative relaxation processes can now dominate, and the long red tail can result in weak absorbance in the NIR. These features of type II dots contrast to those of a type I core−shell structure, where the electron and hole are both confined to the core, which leads to faster radiative lifetimes and a smaller spectral shift between absorption and emission. Here we present an alternative to the II−VI type II dots with type I dots based on the III−V family. The QDs presented here are engineered to emit in the desirable 800 nm range with a quantum yield (QY) and absorption cross section that are sufficient for biomedical imaging, and with a hydrodynamic diameter of 10−15 nm that is optimized for SLN mapping. Within the III−V family the choices of materials that can access the NIR are limited to the larger (>6 nm) InP QDs, for which a robust synthesis is lacking, or smaller InAs (<2 nm) QDs which, because of their small size, have an absorbance that is smaller than desired. Our approach, similar to recent work on II−VI ternary alloy QDs,[4] is to use a combination of InP and InAs to have a reasonably sized QD with emission in the NIR. We report here the synthesis of QDs with a core/shell/shell structure consisting of a III−V

[†] Massachusetts Institute of Technology.
[‡] Beth Israel Deaconess Medical Center.
[§] Ajou University.

(1) (a) Coe, S.; Woo, W.-K.; Bawendi, M. G.; Bulovic, V. *Nature* **2002**, *420*, 800−803. (b) Bruchez, M., Jr.; Moronne, M.; Gin, P.; Weiss, S.; Alivisatos, A. P. *Science* **1998**, *281*, 2013−2015. (c) Huynh, W. U.; Dittmer, J. J.; Alivisatos, A. P. *Science* **2002**, *295*, 2425−2427. (d) Klimov, V. I.; Mikhailovsky, A. A.; Xu, S.; Malko, A.; Hollingsworth, J. A.; Leatherdale, C. A.; Eilser, H.-J.; Bawendi, M. G. *Science* **2000**, *290*, 314−317.
(2) (a) Guzelian, A. A.; Banin, U.; Kadavanich, A. V.; Peng, X.; Alivisatos, A. P. *Appl. Phys. Lett.* **1996**, *69*, 1432−1434. (b) Peng, X.; Wickham, J.; Alivisatos, A. P. *J. Am. Chem. Soc.* **1998**, *120*, 5343−5344. (c) Cao, Y. W.; Banin, U. *J. Am. Chem. Soc.* **2000**, *122*, 9692−9702. (d) Peng, X.; Battaglia, D. *Nano Lett.* **2002**, *2*, 1027−1030.
(3) (a) Kim, S.; Lim, Y. T.; Soltesz, E. G.; De Grand, A. M.; Lee, J.; Nakayama, A.; Parker, J. A.; Mihaljevic, T.; Laurence, R. G.; Dor, D. M.; Cohn, L. H.; Bawendi, M. G.; Frangioni, J. V. *Nature Biotechnol.* **2004**, 22, 93−97. (b) Parungo, C. P.; Ohnishi, S.; Kim, S.-W.; Kim, S.; Laurence, R. G.; Soltesz, E. G.; Chen, F. Y.; Colson, Y. L.; Cohn, L. H.; Bawendi, M. G.; Frangioni J. V. *J. Thorac. Cardiovasc. Surg.* **2005**, *129*, 844−850.
(4) (a) Nie, S.; Bailey, R. E. *J. Am. Chem. Soc.* **2003**, *125*, 7100−7106. (b) Tsay, J. M.; Pflughoefft, M.; Bentolila, L. A.; Weiss, S. *J. Am. Chem. Soc.* **2004**, *126*, 1926−1927. (c) Zhong X.; Feng, Y.; Knoll, W.; Han, M. *J. Am. Chem. Soc.* **2003**, *125*, 13559−13563.

10.1021/ja0434331 CCC: $30.25

graded alloy core of $InAs_xP_{1-x}$, an intermediate shell of InP, and an outer shell of ZnSe. The purpose of the shells is to increase the quantum yield and stability of the QDs. We disperse these QDs in water using a previously described oligomeric phosphine ligand.[5] We chose to engineer these dots with an alloyed core to simultaneously satisfy the size and emission wavelength requirements for this application, demonstrating the flexibility inherent in the colloidal synthesis of quantum dots. The goal in designing QDs for this application is to maximize the volume of the absorbing inorganic core, and hence to maximize its absorption cross section.

Experimental Section

Materials. Indium acetate ($In(Ac)_3$, 99.99%) and selenium shot (Se, 99.999%) were purchased from Alfa Aesar. Tri-*n*-octylphosphine (TOP, 97%), tris(trimethylsilyl)phosphine ($(TMS)_3P$, 98%), and diethylzinc (Et_2Zn, 95%) were purchased from Strem. Diethylzinc was filtered through a 0.2 μm filter in an inert atmosphere box. Octadecene (90%) was purchased from Aldrich. Oleic acid (99%) was purchased from TCI. A TOP−Se solution (1 M) was prepared by dissolving 7.90 g of selenium shot in 100 mL of TOP, yielding a colorless solution. Tris(trimethylsilyl)arsine was synthesized according to the literature procedure.[6]

Characterization. Absorbance and photoluminescence were measured on a HP-8453 spectrophotometer and a SPEX Fluorolog-2 spectrofluorimeter, respectively. Dilute solutions of dots in hexane were placed in 1 cm quartz cuvettes, and their absorption and corresponding fluorescence were measured. The room-temperature quantum yields (QY) were measured by comparing the integrated emission of the dots in solution to the emission of a solution of HITC (Exciton, QY = 28% in MeOH) in methanol as a standard. Transmission electron micrographs and high-resolution transmission electron micrographs were obtained on JEOL 2000 and 2010 electron microscopes operated at 200 kV, respectively. Elemental analysis data were obtained using wavelength-dispersive spectroscopy (WDS) on a JEOL JXA-733 Superprobe. Thick films of QDs were drop-cast from concentrated hexane solutions onto Si(100) wafers, and after the solvent had completely evaporated, the films were coated with a thin layer of amorphous carbon to prevent charging. Powder X-ray diffraction (PXRD) patterns were obtained on a Rigaku Ru300 X-ray diffractometer. Samples for PXRD were obtained by drop-casting solutions of QDs onto low-scattering quartz plates and evaporating the solvent under vacuum. Gel filtration was performed on a Biological LP system using Sephacryl S-400 resin (Sigma) and an XK 16/20 column (Amersham). Quasi-elastic light scattering (QELS) was performed on a model 90 Plus particle size analyzer (Brookhaven Instrument).

Fabrication of Alloyed $InAs_xP_{1-x}$ Quantum Dots. To make $InAs_{0.66}P_{0.33}$, 0.044 g (0.15 mmol) of indium acetate and 0.127 mg (0.45 mmol) of oleic acid were added to 8 mL of octadecene and degassed at 120 °C for 1 h. The solution was purged with nitrogen and then heated to 300 °C under nitrogen. Next, 0.0125 g (0.05 mmol) of $(TMS)_3P$ and 0.0147 g (0.05 mmol) of $(TMS)_3As$ were dissolved in 2 mL of octadecene in a glovebox and injected into the hot reaction flask. After injection, the temperature was dropped to 270 °C, which was maintained for 1 h. The solution was cooled to room temperature, and the dots were then precipitated with an excess of ethanol. The same procedure is used to prepare $InAs_{0.33}P_{0.66}$ and $InAs_{0.82}P_{0.18}$ dots, except that 0.018 g (0.075 mmol) of $(TMS)_3P$ and 0.007 g (0.025 mmol) of $(TMS)_3As$ were used for the $InAs_{0.33}P_{0.66}$ dots, and 0.006 g (0.025 mmol) of $(TMS)_3P$ and 0.022 g (0.075 mmol) of $(TMS)_3As$ were used for the $InAs_{0.82}P_{0.18}$ dots.

In Situ Fabrication of $InAs_{0.82}P_{0.18}$/InP Core−Shell Quantum Dots. The growth solution of $InAs_{0.82}P_{0.18}$ at 270 °C in the previous section was cooled to 140 °C instead of room temperature. Next, 0.030 g (0.10 mmol) of indium acetate and 0.018 g (0.075 mmol) of $(TMS)_3P$ were combined with 2 mL of octadecene in a glovebox. This mixture was injected into the solution of dots, and the temperature was increased to 180 °C, which was maintained for 1 h. The same procedure was also used for the second injection of In and P precursors (cooling to 140 °C, injecting, increasing the temperature to 180 °C for 1 h).

In Situ Fabrication of $InAs_{0.82}P_{0.18}$/InP/ZnSe Core−Shell Quantum Dots. The growth solution of $InAs_{0.82}P_{0.18}$/InP dots, maintained at 180 °C for 1 h in the previous section, was heated from 180 to 200 °C. Next, 0.024 g (0.20 mmol) of Et_2Zn and 0.2 mL (0.20 mmol) of 1 M TOP−Se were combined in 2 mL of TOP in a glovebox. This mixture was add dropwise for 1 h into the solution of dots at 200 °C. The solution of dots was cooled to room temperature, and the dots were precipitated out of solution with ethanol and dried in air.

Etching of $InAs_{0.66}P_{0.33}$ Alloyed QDs. First, 2 mL of *n*-BuOH and 2 mL of 1 N HCl solution were added to a 10 mL vial which contained 10 mg of precipitated and dried QDs. This solution was sonicated for 1 or 2 min, yielding a two-phase solution consisting of a colored upper phase of butanol and dots, and a lower phase of a colorless HCl solution. The HCl solution was removed. Ethanol was added to the remaining upper phase, yielding a colored precipitate and a colorless supernatant. The supernatant was discarded and the precipitate redissolved in THF, yielding a colored solution of dots and a small amount of white insoluble material. The THF solution was then used for WDS and TEM measurements.

Cap Exchange. A large excess of oligomeric phosphine, synthesized according to ref 4, was stirred with the QDs in THF for 1 h. The solvent was removed at a reduced pressure, and the dot/oligomeric phosphine mixture was maintained at 100 °C for 1 h and then cooled to room temperature. Next, 50 mL of 1 N NaOH was added, and the solution was stirred vigorously at room temperature, forming a dark brown basic solution. Ten equivalent volumes of a PBS buffer solution (pH 7.0) was added, and the solution was dialyzed using a centrifugal filter device (50 kDa, Millipore). This procedure was repeated five times to remove excess oligomeric phosphine cap. The solution was then finally filtered using a 0.1 μm PTFE disposable filter (Nalgene).

Sentinel Lymph Node Mapping. The NIR fluorescence imaging system has been described elsewhere in detail.[7] Briefly, it is composed of two light sources, a NIR fluorescence excitation light (725−775 nm, 5 mW/cm^2) to excite the NIR fluorophore and a white light (400−700 nm, 0.5 mW/cm^2) for imaging in the visible. White light images and images of the NIR fluorescence can be displayed separately and merged. The entire apparatus is suspended on an articulated arm over the surgical field, thus permitting noninvasive and nonintrusive imaging. Real-time video images, refreshed 15 times per second, and zooming capability allowed precise localization and dissection as needed. For surgery, rats were anesthetized with 75 mg/kg intraperitoneal pentobarbital. Next, 150 pmol of QDs in 0.1 mL of PBS buffer (pH 7.0) solution were injected subdermally and observed with an imaging instrument.

Result and Discussion

The synthetic procedure for the alloyed core is inspired by ref 2d for InP and InAs QDs, with indium acetate ($In(OAc)_3$), tris(trimethylsilyl)phosphine ($(TMS)_3P$), and tris(trimethylsilyl)-arsine ($(TMS)_3As$) as indium, phosphorus, and arsenic precursors, respectively. The phosphorus and arsenic precursors were injected into a solution of $In(OAc)_3$ and oleic acid in 1-octadecene. To study the growth process and stoichiometry of the

(5) Kim, S.; Bawendi, M. G. *J. Am. Chem. Soc.* **2003**, *125*, 14652−14653.
(6) Becker, G.; Gutekunst, G.; Wessely, H. *Z. Anorg. Allg. Chem.* **1980**, *462*, 113−129.
(7) (a) De Grand, A. M.; Frangioni, J. V. *Technol. Cancer Res. Treat.* **2003**, *2*, 553−562. (b) Zaheer, A.; Lenkinski, R. E.; Mahmood, A.; Jones, A. G.; Cantley, L. C.; Frangioni, J. V. *Nat. Biotechnol.* **2001**, *19*, 1148−1154.

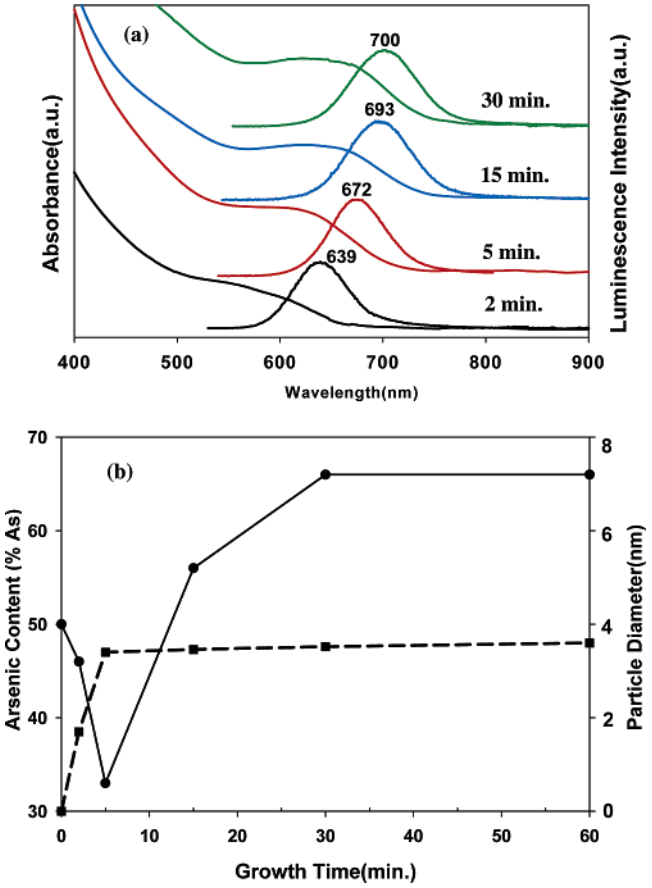

Figure 1. Temporal evolution of (a) absorption and emission spectra and (b) arsenic content (solid line) and particle size (dashed line) for $InAs_{0.66}P_{0.33}$ QDs.

growing alloyed dots, aliquots of the reaction solution were removed at 2, 5, 15, and 30 min. Absorption and emission spectra, TEM, and WDS were used to characterize the growing dots. Figure 1a shows the absorption and emission spectra of $InAs_{0.66}P_{0.33}$ dots (the notation uses the final stoichiometry according to WDS) versus time. The growth occurs gradually over 30 min of reaction time, as seen by the increasing red-shift in Figure 1. An As-to-P precursor ratio of 50/50 is found to yield a final dot composition with an As-to-P ratio of 66/33. The kinetic data for the temporal evolution of the stoichiometry and particle size are shown in Figure 1b. WDS and TEM data at the 2 min mark show an As-to-P ratio of 47/53 and 1.7 nm diameter dots, indicating that both precursors nucleate at roughly the same rate. The data at the 5 min mark gives a 33/66 As-to-P ratio and 3.5 nm diameter dots, showing that growth is largely due to the formation of InP, indicating faster growth reaction kinetics for the phosphine precursor compared to the arsenic precursor. The data at the 15 min mark give an As-to-P ratio of 56/44 and 3.6 nm diameter dots, showing a significant change in the composition with almost no change in size, implying an exchange between the phosphorus in the dots with the arsenic still in the solution. Previous studies on bulk semiconductors have demonstrated exchange of phosphorus with arsenic; when an InP surface is exposed to an arsenic-bearing ambient gas, the result is a graded alloy with the highest arsenic content at the surface.[8] Anan et al. reported that the phosphorus

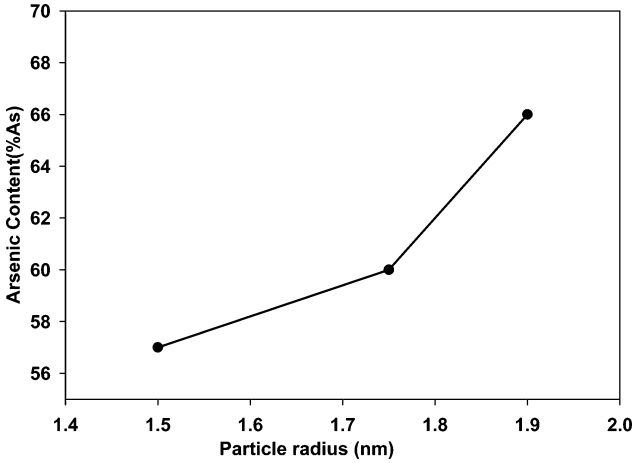

Figure 2. Arsenic content of $InAs_{0.66}P_{0.33}$ alloyed QDs with etching.

in InP can be replaced by arsenic but not vice versa,[9] and Gong et al. explained this on the basis of the chemical bond strength difference of arsenic and phosphorus to indium[10] (In−As bonds, with a bond strength of 48.0 kcal/mol, are slightly more stable than In−P bonds, at 47.3 kcal/mol). The red-shift observed in Figure 1 from the 2−5 min mark (33 nm) is due to growth, while the red-shift from the 5−15 min mark (21 nm) results from the change in stoichiometry as the As content increases. The internal stoichiometry of the dots is further clarified by chemically etching $InAs_{0.66}P_{0.33}$ alloyed dots with a solution of 1 N HCl and *n*-BuOH. The arsenic composition is observed to change from 66% for the 3.8 nm dots to 60% and then 53% as the dots are etched down to 3.5 and 3 nm, respectively, indicating a graded composition that is richer in arsenic close to the surface of the dot (Figure 2).

Elemental analyses by WDS show that the dots are consistently richer in As/P ratio than the precursor solution; As-to-P ratios of 75/25, 50/50, and 25/75 result in dot compositions with As-to-P ratios of 82/18, 66/33, and 33/66, respectively. TEM images show that the dots are crystalline and are of a similar size (Figure 3a, for $InAs_{0.66}P_{0.33}$, $d_{av} = 3.77$ nm, $\sigma = 0.65$ nm; Figure 3b, for $InAs_{0.33}P_{0.66}$, $d_{av} = 4.23$ nm, $\sigma = 0.81$ nm, and for $InAs_{0.82}P_{0.18}$, $d_{av} = 4.02$ nm, $\sigma = 0.87$ nm). Pure InP and InAs dots synthesized with this method give sizes that are ∼3 nm and <2 nm, respectively. Powder X-ray diffraction (XRD) patterns exhibit three prominent peaks, indexed to the scattering from the (111), (220), and (311) planes of the zinc blend structure of the ternary alloy dots over all compositions (Figure 4). It is not possible to distinguish between a homogeneous alloy and a graded structure on the basis of the XRD patterns because the peaks are too broad. The alloy dots are easily oxidized to In_2O_3, as shown by the (222) reflection at 31° and the (400) reflection at 35°.[11] Absorption and fluorescence spectra of alloy dots with varying arsenic content are shown in Figure 5. Changing the arsenic-to-phosphorus ratio while keeping the size roughly constant tunes the emission from ∼600 to ∼800 nm. Increasing the reaction time to 3 h does not shift the emission bands of the pure InP dots or of the alloy dots, but the emission band of the pure InAs dots is shifted to 800 nm. The wide full width at half-maximum (fwhm) of the emission band is

(8) Carlsson, N.; Junno, T.; Montelius, L.; Pistol, M.-E.; Samulelson, L.; Seifert, W. *J. Cryst. Growth* **1998**, *191*, 347−356.
(9) Anan, T.; Sugou, S.; Nishi, K. *Appl. Phys. Lett.* **1993**, *63*, 1047−1049.
(10) Gong, Q.; Notzel, R.; Veldhoven, P. J. V.; Eijkemans, T. J.; Wolter, J. H. *Appl. Phys. Lett.* **2004**, *84*, 275−277.
(11) Girtan, M. *Surf. Coat. Technol.* **2004**, *184*, 219−224.

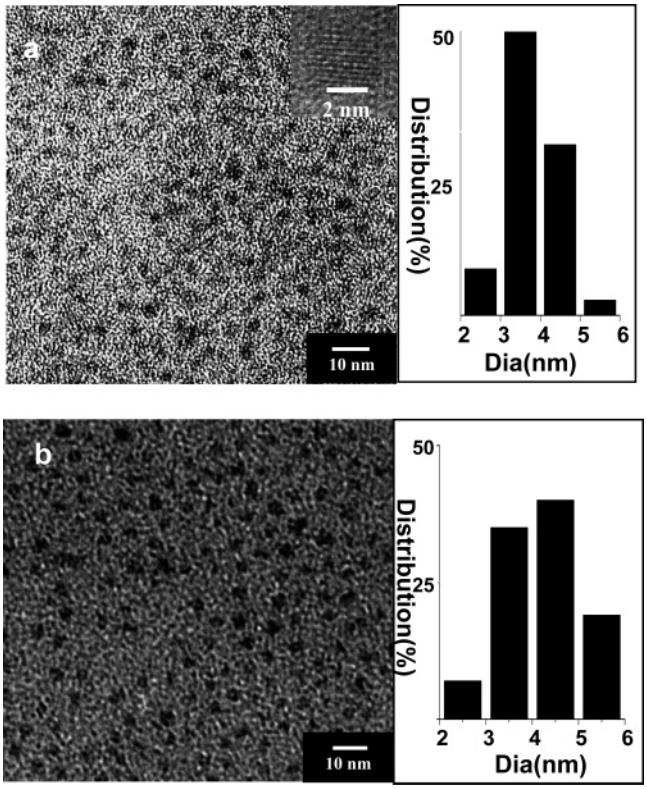

Figure 3. TEM images of (a) $InAs_{0.66}P_{0.33}$ and (b) $InAs_{0.33}P_{0.66}$ QDs.

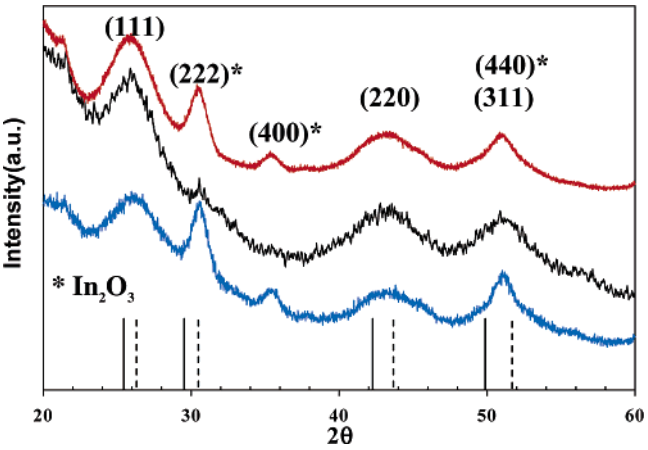

Figure 4. Powder XRD patterns of $InAs_xP_{1-x}$ alloyed QDs; solid ticks are for bulk InAs and dotted ticks are for bulk InP. The red line is for $InAs_{0.82}P_{0.18}$ QDs, the black line is for $InAs_{0.66}P_{0.33}$ QDs, and the blue line is for $InAs_{0.33}P_{0.66}$ QDs.

characteristic of the III−V family, which results from an effective electron mass which is significantly lighter than in the II−VI family. Figure 6 plots the peak position of the emission from alloy dots (solid line) and the band gap of the bulk alloy (dashed line)[12] as a function of arsenic mole ratio. These have a similar shape despite the graded composition of the dots. As with other III−V allows, Vegard's law is not obeyed.[12] The alloy dots prior to further treatment have a quantum yield of 1−2%.

The alloyed dot cores were overcoated with a shell of InP to increase their size and QY. This shell was grown by injecting

(12) (a) Swaminathan, V.; Macrander, A. T. *Materials Aspects of GaAs and InP based Structures*; Prentice Hall: Englewood Cliffs, NJ, 1991. (b) http://www.ee.byu.edu/cleanroom/EW_ternary.phtml

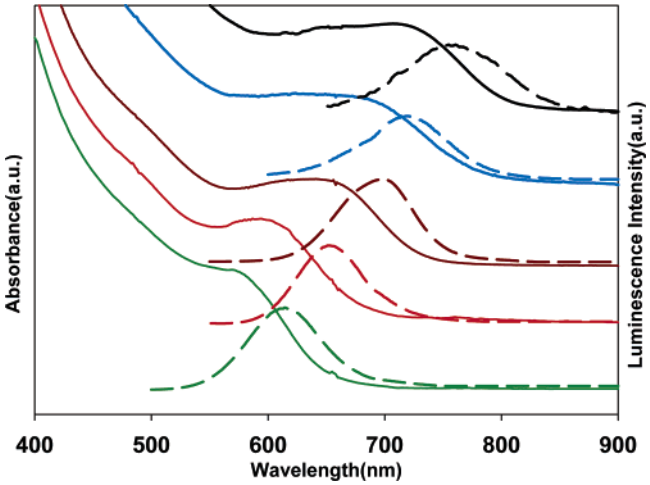

Figure 5. Absorbance (solid line) and corresponding photoluminescence (dashed line) for QDs of InP (emission 614 nm, fwhm 74 nm), $InAs_{0.33}P_{0.66}$ (emission 652 nm, fwhm 68 nm), $InAs_{0.66}P_{0.33}$ (emission 699 nm, fwhm 81 nm), $InAs_{0.82}P_{0.18}$ (emission 738 nm, fwhm 86 nm), and InAs (emission 755 nm, fwhm 105 nm), from bottom to top, respectively.

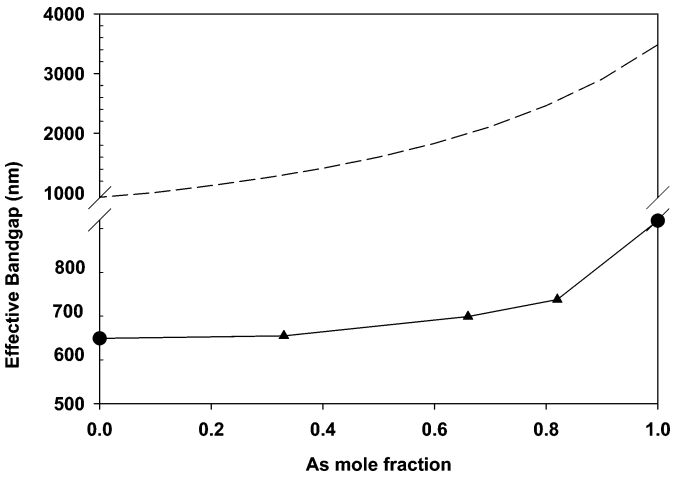

Figure 6. Plot of band gap of bulk materials (dashed line, ref 11) and the emission peak wavelength as a function of arsenic content (solid line); experimental (▲) and extrapolated from refs 16 (InP) and 2a (InAs) (●).

a mixture of $In(OAc)_3$ and $(TMS)_3P$ to the solution of alloyed dots at 140 °C, low enough to avoid nucleation. The temperature was then increased to 180 °C to initiate shell growth. Two successeive injections of In and P precursors, both at 140 °C, to a solution of $InAs_{0.82}P_{0.18}$ (738 nm fluorescence peak) QDs resulted in core−shell particles with emission at 765 nm after the first injection (fwhm 103 nm) and 801 nm after the second injection (fwhm 119 nm) (Figure 7) and a tripling of the QY. Although this core−shell is of type I, a large red-shift of the effective band gap with growth of the shell is nevertheless observed. Figure 8 shows a potential energy diagram for $InAs_{0.82}P_{0.18}$/InP core−shell QDs and the result of a simple model for the radial probability distribution function for electron and hole wave functions in the lowest energy state.[13] Qualitatively, we find that the electron wave function penetrates into the InP shell while the hole wave function has a negligible

(13) Dabbousi, B. O.; Rodriguez-Viejo, J.; Mikulec, F. V.; Heine, J. R.; Mattoussi, H.; Ober, R.; Jensen, K. F.; Bawendi, M. G. *J. Phys. Chem. B* **1997**, *101*, 9463. Effective electron and hole masses for InAs used were $m_e^* = 0.023m_e$ and $m_h^* = 0.57m_e$, where m_e is the mass of the free electron (Madelung, O. *Semiconductors: Data Handbook*; Springer: Berlin, 2004).

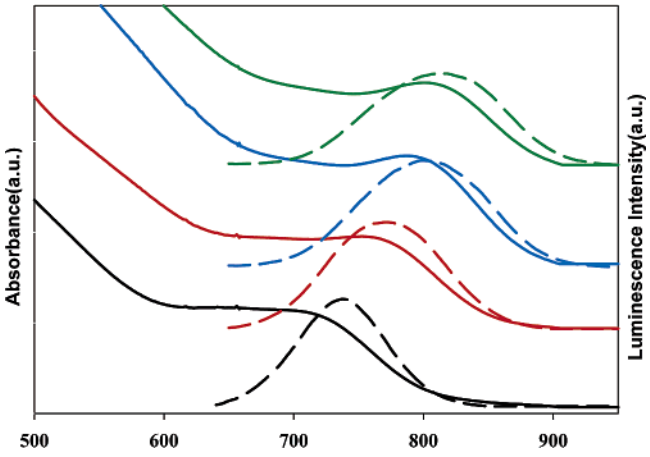

Figure 7. Absorbance (solid line) and corresponding photoluminescence (dashed line) spectra of core $InAs_{0.82}P_{0.18}$ QDs (emission 738 nm, fwhm 86 nm), after a first shell of InP (emission 765 nm, fwhm 103 nm), after a second shell of InP (emission 801 nm, fwhm 119 nm), and after the final ZnSe shell (emission 815 nm, fwhm 120 nm), from bottom to top, respectively.

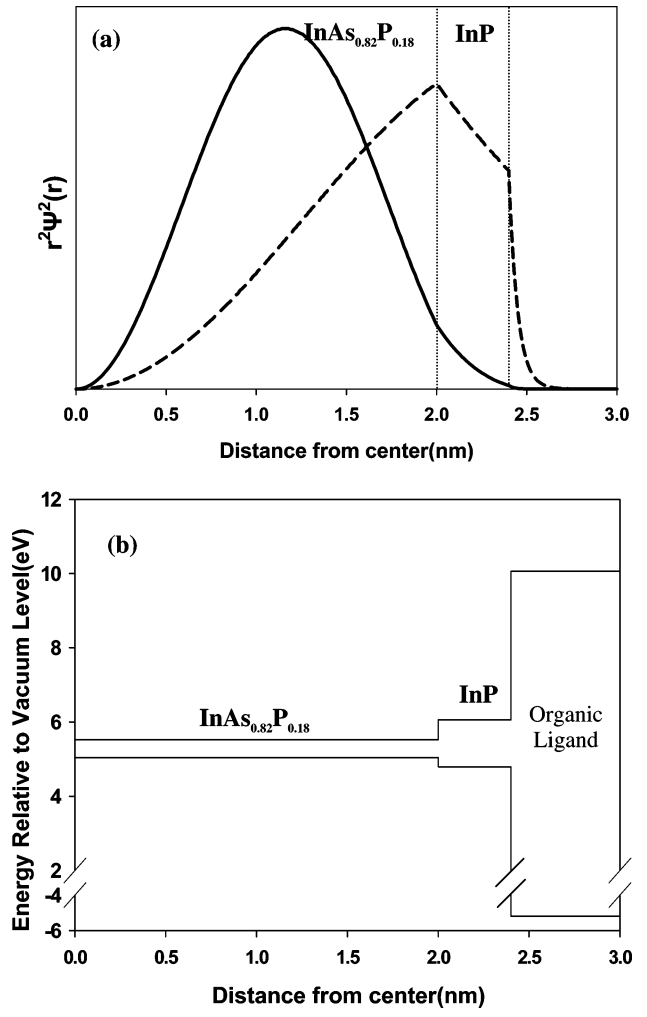

Figure 8. Modeled (a) radial distribution functions for electron (dashed line) and hole (solid line) wave functions in the lowest energy and (b) potential diagram of 2 nm alloy core and 0.4 nm thickness shell.

probability of spreading into the InP layer. The increased delocalization of the electron lowers its confinement energy and the energy of the excited state, leading to the observed red-shift with increasing shell thickness. TEM images confirm the

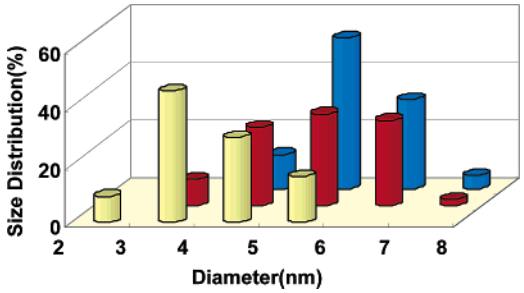

Figure 9. Histograms of particle size distributions for $InAs_{0.82}P_{0.18}$ core (yellow), $InAs_{0.82}P_{0.18}$/InP core−shell (red), and $InAs_{0.82}P_{0.18}$/InP/ZnSe core/shell/shell (blue) QDs.

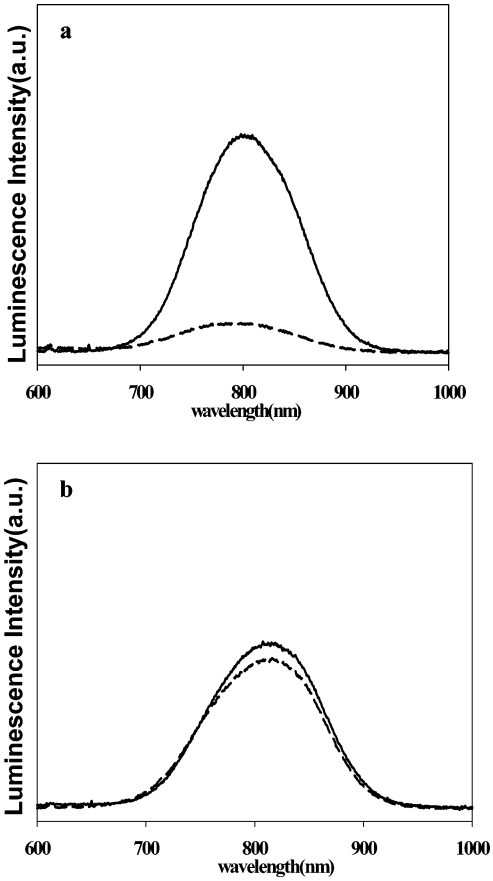

Figure 10. (a) Photoluminescence of $InAs_{0.82}P_{0.18}$/InP core/shell QDs in hexane (solid line) and PBS buffer (pH 7.0) (dashed line). (b) Photoluminescence of $InAs_{0.82}P_{0.18}$/InP/ZnSe core/shell QDs in hexane (solid line) and PBS buffer (pH 7.0) (dashed line).

shell growth, as shown in the histogram of Figure 9. The shell growth temperature is low enough that no exchange of phosphorus with arsenic is observed. At this stage, cap exchange with oligomeric phosphines can impart water solubility to the QDs, but with a QY that is decreased by 90%, likely due to the ease of oxidation of III−V QDs (Figure 10a).

Stabilizing the dots for dispersal in aqueous solution was initially attempted with a ZnS shell, but this was not successful. We instead succeeded with ZnSe, maybe because of its better lattice match to InP. Adding a trioctylphosphine (TOP) solution of diethylzinc (Et_2Zn) and trioctylphosphine selenide (1 M TOP−Se in TOP) dropwise to a solution of $InAs_{0.82}P_{0.18}$/InP dots over 1 h at 200 °C resulted in an additional red-shift of 10−15 nm in the emission peak. Figure 7 shows an example of such a sample emitting at 815 nm (fwhm 120 nm) with a

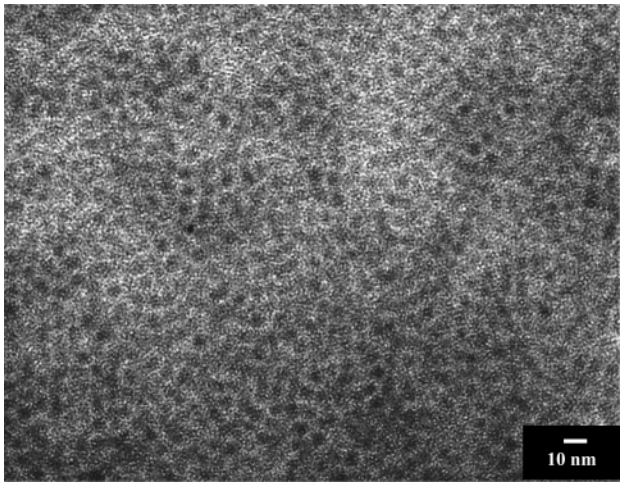

Figure 11. TEM image of $InAs_{0.82}P_{0.18}$/InP/ZnSe core−shell QDs.

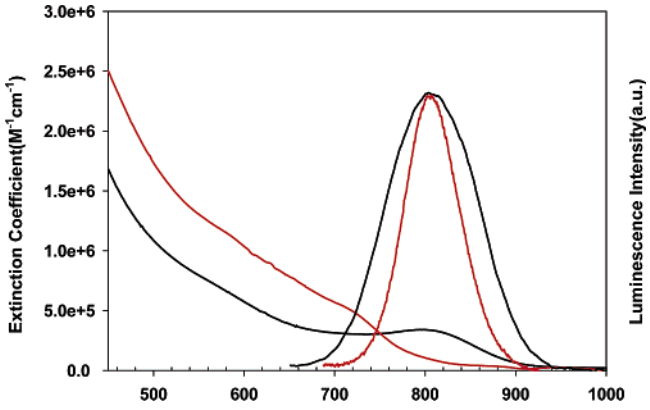

Figure 12. Molar extinction coefficient (left axis) and photoluminescence intensity (PL) (right axis) of alloyed dots (black) and type II dots (red) in hexane. The PL intensities for the two samples are scaled for comparison of their peak wavelengths and do not reflect absolute intensities.

QY of 3.5% (twice the QY of the alloy core). The histogram of Figure 9 shows the additional shell growth. Figure 11 shows a TEM micrograph from this same sample ($d_{av} = 5.78$ nm, $\sigma = 0.74$ nm). Cap exchange with oligomeric phosphines and transfer to water did not have an appreciable effect on the QY (Figure 10b). The QY, although low, is large enough for biomedical imaging experiment and competitive with the previously described type II QDs because the absorption spectrum of the alloyed type I QDs has a peak in the important NIR region instead of the characteristic red tail of type II QDs, meaning that the effective brightness is similar for those two types of dots. For example, at 775 nm, the extinction coefficient of alloyed core−shell QDs that emit at 805 nm is approximately twice that of type II QDs that also emit at 805 nm (Figure 12). In addition, in an application such as SLN mapping, the total volume of QDs may actually be more important than the number of QDs in the SLN. The type II dots, at 9 nm in diameter (for the inorganic portion), have roughly 3 times the inorganic volume of the 6 nm diameter dots in the present study. On an equal volume basis, the present dots therefore roughly absorb at least 6 times more light in the NIR than the previous type II dots. This increased fraction of absorbed excitation photons easily makes up for the lower quantum yield. It is also useful to recall that quantum yields of new QD formulations historically do tend to increase as reaction phase space is explored over time.

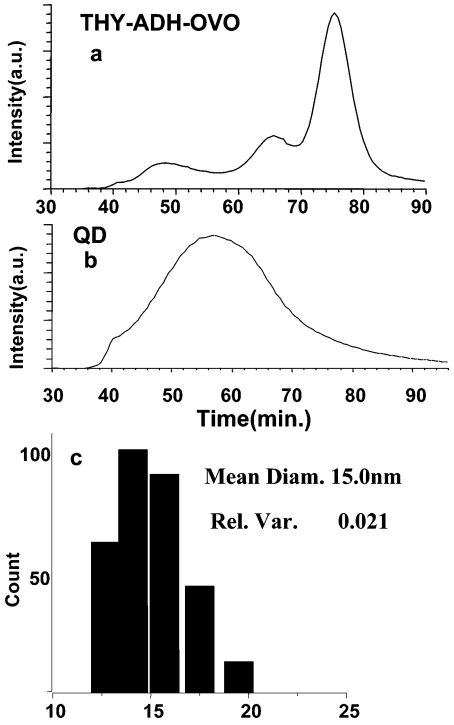

Figure 13. Gel filtration chromatography of (a) protein standards thyroglobulin (THY, 669 kDa, 48.3 min), alcohol dehydrogenase (ADH, 150 kDa, 65.7 min), and ovalbumin (OVO, 44 kDa, 75.4 min), and (b) $InAs_{0.82}P_{0.18}$/InP/ZnSe core/shell/shell QDs (230 kDa, 57.2 min) in PBS buffer (pH 7.0). (c) Quasi-elastic light scattering (QELS) data for $InAs_{0.82}P_{0.18}$/InP/ZnSe core/shell/shell QDs in PBS buffer (pH 7.0).

The hydrodynamic diameter of the final product is important to SLN mapping because species between 5 and 10 nm can flow through the SLN and into subsequent nodes in the chain, and species >300 nm do not leave the injection site.[14] Alloyed core/shell/shell QDs stabilized with oligomeric phosphines ran equivalently to a protein of 230 kDa in gel filtration, corresponding to a hydrodynamic diameter of approximately 12 nm (Figure 13). The hydrodynamic diameter measured by quasi-elastic light scattering (QELS) was 15 nm (Figure 13c). We have demonstrated the applicability of these new QDs in an SLN mapping experiment. We used an intraoperative video imaging system that superimposes NIR fluorescence on a display of visible light anatomy. When injected intradermally into the paw of a mouse, the small amount and low concentration of NIR QDs injected cannot be seen on the color video images (Figure 14a). However, the fluorescence image (Figure 14b,e) reveals the fine detail of lymphatic flow from the injection site to the SLN. Background autofluorescence from tissue is low in this spectral region, permitting a high signal-to-background ratio. Injected QDs entered the lymphatics and migrated within 1 min to the sentinel node, which was easily detected through the skin using our intraoperative imaging system (Figure 14).

While the alloyed III−V QDs presented here do not contain cadmium, they include other heavy metals. Some of these, such as selenium, zinc, and phosphorus, are found in minerals and vitamins that are beneficial to humans in small quantities. Others, however, such as indium and arsenic, are heavy metals considered potentially deadly toxins. No toxicity data exist on the toxicity of precomplexed dots injected subdermally. Without

(14) Uren, R. F.; Hoefnagel, C. A. In *Textbook of Melanoma*; Thompson, J. F., Morton, D. M., Kroon, B. B. R., Eds.; Martin Dunitz: London, 2003.

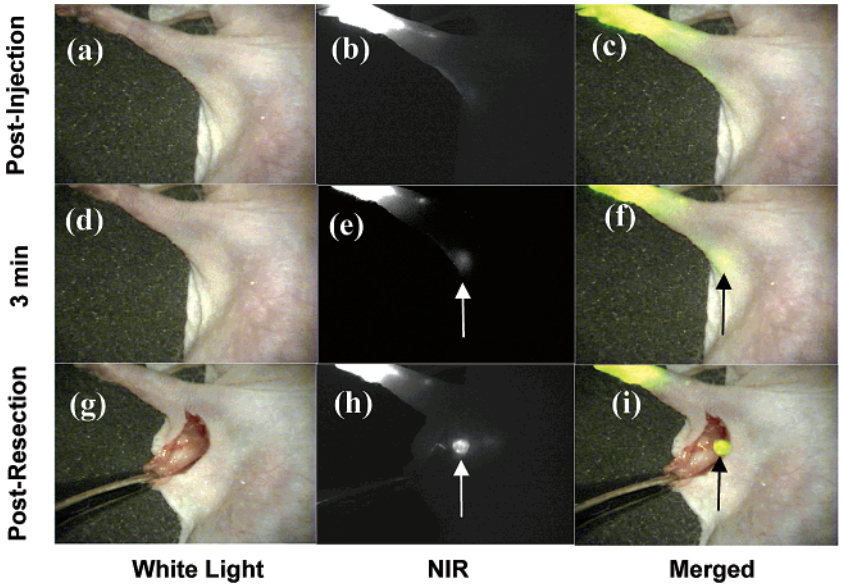

Figure 14. Postinjection (a, b, c), 3 min postinjection (d, e, f), and post-resection (g, h, i) images using white light, NIR fluorescence, and color/NIR merge, respectively.

such data, we can only speculate. In sentinel lymph node mapping using III−V NIR QDs, 150 pmol of injected QDs contains 5 μg of arsenic and 22 μg of indium. While the amount that would ultimately be required in an optimized experiment for SLN imaging in a human is not known, this amount of As is hundreds of times lower than the dose of As_2O_3 used to treat human leukemia. In addition, an average American ingests on the order of 10 μg of inorganic arsenic and ~10 μg of indium daily from food and water.[15] It is possible, therefore, that despite being composed of potentially toxic materials, the dosage may be small enough that overall toxicity is low.

In summary, we have developed quantum dots with a core/shell/shell structure consisting of an alloy core of $InAs_{1-x}P_x$, an intermediate shell of InP, and an outer shell of ZnSe. Alloyed core dots of $InAs_xP_{1-x}$ show tunable emission in the NIR region, and the InP shell leads to a red-shift and an increase in the quantum yield. The ZnSe shell imparts stability in water. Core/shell/shell dots of $InAs_xP_{1-x}$/InP/ZnSe dots dispersed in water were successfully used in NIR sentinel lymph node mapping experiments.

Acknowledgment. This work was supported by the Korean Science & Engineering Foundation postdoctoral fellowship program, and by NIH grant R33 EB-00673.

JA0434331

(15) Goyer, R. A.; Clarkson, T. W. In *Toxicology*; Klaassen, C. D., Ed.; McGraw-Hill: New York, 2001.

(16) Talapin, D. V.; Gaponik, N.; Borchert, H.; Rogach, A. L.; Haase, M.; Weller, H. *J. Phys. Chem. B* **2002**, *106*, 12659−12663.